Molecular Basis of Metal-Ion Selectivity and Zeptomolar Sensitivity by CueR

Anita Changela,[1]* Kui Chen,[2]* Yi Xue,[2] Jackie Holschen,[2] Caryn E. Outten,[2] Thomas V. O'Halloran,[1,2]† Alfonso Mondragón[1]†

The earliest of a series of copper efflux genes in *Escherichia coli* are controlled by CueR, a member of the MerR family of transcriptional activators. Thermodynamic calibration of CueR reveals a zeptomolar (10^{-21} molar) sensitivity to free Cu^+, which is far less than one atom per cell. Atomic details of this extraordinary sensitivity and selectivity for +1 transition-metal ions are revealed by comparing the crystal structures of CueR and a Zn^{2+}-sensing homolog, ZntR. An unusual buried metal-receptor site in CueR restricts the metal to a linear, two-coordinate geometry and uses helix-dipole and hydrogen-bonding interactions to enhance metal binding. This binding mode is rare among metalloproteins but well suited for an ultrasensitive genetic switch.

E. coli maintain a strict cellular copper quota within a narrow range, about 10^4 atoms per cell (~10 μM), by using numerous copper homeostasis pathways to control and allocate the metal to a few important enzymes (*1*, *2*). One of the first responses of *E. coli* to even mild copper stress is the expression of the efflux pump CopA, a homolog of the Menkes and Wilson disease proteins, which removes Cu^+ from the cytosol into the periplasm (*3*, *4*). Copper-induced expression of CopA and CueO, an oxidase postulated to catalyze the air oxidation of Cu^+ to the less toxic Cu^{2+} form in the periplasm (*5*, *6*), is controlled by CueR (*3*, *7*–*9*), a member of the MerR family of metalloregulatory proteins. This family includes metal-responsive transcriptional activators such as the zinc sensor ZntR (*1*, *10*) and the mercury sensor MerR (*11*).

Similar to other MerR metalloregulatory family members, CueR exhibits a metal-selective behavior in vivo, activating the transcription of *copA* in response to elevated extracellular concentrations of the salts of coinage metals, such as copper, silver, and gold, but not of zinc and mercury (*7*–*9*, *12*). Such selectivity can derive either from cellular components (i.e., metallochaperones or transporters) that control metal accessibility to CueR or from the intrinsic metal-recognition properties of CueR itself. To address the molecular basis of this selectivity, we thermodynamically calibrated CueR in an in vitro metal-responsive transcriptional switching assay using well-defined copper-metal–buffering systems. Various metal salts were titrated into run-off transcription assays, in which purified CueR regulates RNA polymerase (RNAP) transcription at the P_{copA} promoter (*13*). Initial studies of CueR show a lack of metal-dependent transcriptional activation: The switch is "on" without addition of any metal ions, even in the presence of high concentrations of avid Cu^+-binding ligands such as glutathione (GSH) (*14*, *15*) (fig. S1). Transcriptional activation by CueR is suppressed only when millimolar concentrations of cyanide (CN^-), which has a higher affinity for Cu^+ than has glutathione (*14*, *16*), are added to the assays. Transcription can be recovered upon the addition of Cu^+ back to the cyanide-containing assays, thus indicating that copper binding to CueR is tight but reversible under these conditions.

Titration of different metals in the presence of 1.0 mM cyanide (Fig. 1A) reveals transcriptional-activation profiles that reproduce the in vivo behavior of the CueR/promoter system (*7*, *9*, *12*). Transcript levels rise steadily with increasing amounts of Cu^+, reaching saturation at 50 μM total Cu^+. Titrations with either Ag^+ or Au^+ ions in the presence of 1.0 mM CN^- gave similar CueR-response profiles (Fig. 1A). Consistent with in vivo results (*9*), neither Hg^{2+} nor Zn^{2+} induced any CueR-mediated transcription in vitro (Fig. 1A). Indeed, little direct binding of Hg^{2+} or Zn^{2+} to CueR is observed when competitors such as dithiothreitol (DTT) are present (*17*). The parallels between the in vivo and the in vitro studies indicate that CueR is capable of directly distinguishing metal ions with a +1 charge from metal ions with a +2 charge in gene regulation.

To calibrate the Cu^+ response profile of CueR, we designed additional transcription assays under a series of metal-buffering conditions that precisely control the free Cu^+ concentration. Given critical stability constants for the Cu^+/CN^- system, the pK_a of CN^- (where K_a is the acid dissociation constant), and total CN^- concentrations that exceed both copper and protein concentrations (i.e., ≥1.0mM), the free Cu^+ concentration in vitro can be readily buffered at values in the range of 10^{-23} to 10^{-18} M (pH 8.0) (fig. S2) (*16*). Half-maximal CueR induction occurs at a free Cu^+ concentration of $2 \times 10^{-21} \pm 1 \times 10^{-21}$ M, corresponding to a zeptomolar CueR sensitivity for Cu^+ (Fig. 1B). For comparison, the Zn^{2+} sensor, ZntR, exhibits half-maximal induction at a much higher level (1.15×10^{-15} M free Zn^{2+} concentration) (*1*). Considering that the lowest formal intracellular concentration of free copper is $\sim 10^{-9}$ M (i.e., one free copper atom per *E. coli* cell with a volume of 1.5×10^{-15} liter) (*1*), the CueR switch is tripped at a copper concentration that is formally 11 orders of magnitude lower than one free Cu^+ atom per cell. This thermodynamic result indicates that Cu^+ binds to CueR much more tightly than to glutathione, the most abundant thiol in the cell, and is consistent with the observation that GSH alone is not a reasonable competitor for Cu^+ in the CueR activation of P_{copA} (fig. S1). These results lead us to propose that neither free Cu^+ nor copper-glutathione complexes constitute a persistent "copper pool" in the prokaryotic cytosol under normal growth conditions.

To understand metal sensitivity and selectivity in the MerR family of metalloregulatory proteins at the atomic level, we solved the x-ray crystal structures of metal-bound forms of two representative members that discriminate between metal ions with a +1 and a +2 charge: *E. coli* CueR and *E. coli* ZntR. The structures of Cu^+-, Ag^+-, and Au^+-bound forms of CueR were determined to 2.2, 2.1, and 2.5 Å resolution, respectively, whereas the structure of an N-terminally truncated fragment of ZntR bound to Zn^{2+} was solved to 1.9 Å resolution (*13*). The overall structure of the CueR dimer is identical in all three metal-bound states. Each monomer can be divided into three distinct functional domains: a dimerization domain flanked by a DNA-binding domain and a metal-binding domain (Fig. 2A). The structure of the CueR DNA-binding and dimerization domains is characteristic of the MerR family of proteins and shares the same topology as the structures of two other MerR-family transcriptional activators, BmrR (*18*) and MtaN (*19*, *20*), which respond to the presence of organic substrates.

In each CueR structure, the metal ion is buried in a solvent-inaccessible site in a loop at the dimer interface (Fig. 2B) and has only two coordinating ligands: the S-atoms of con-

[1]Department of Biochemistry, Molecular Biology, and Cell Biology, [2]Department of Chemistry, Northwestern University, 2205 Tech Drive, Evanston, IL 60208, USA.

*These authors contributed equally to this work.
†To whom correspondence should be addressed. E-mail: t-ohalloran@northwestern.edu (T.V.O.) and a-mondragon@northwestern.edu (A.M.)

served Cys[112] and Cys[120] (Fig. 3A). These residues define the end points of a 10-residue loop that extends from the C-terminal end of the dimerization helix up to the N-terminus of a short two-turn α helix. In the dimer, only one metal-binding loop is fully ordered, even though another metal is bound at the equivalent site in the dimer. Residues 115 to 119 of the second monomer are disordered, perhaps due to differences in crystal packing. This disorder suggests that flexibility in the extended region of the metal-binding loop may allow metal access to the buried binding site. The metal-binding loop of one monomer rests against the N-terminal end of the long dimerization helix and the preceding loop of the other monomer, interacting primarily through backbone contacts. The short two-turn α helix that extends from the metal-binding loop packs against the DNA-binding domain of the other monomer and against both dimerization helices by way of several conserved hydrophobic residues (Fig. 3). These extensive hydrophobic interactions effectively form a scaffold that stabilizes the buried metal-binding site.

Coordinate-covalent bonds between the Cu^+ ion and the two sulfur atoms of Cys[112] and Cys[120] exhibit Cu-S bond distances of 2.13 Å with an essentially linear S-Cu-S bond angle of 176° (Fig. 3A). Extended x-ray absorption fine structure studies on copper-CueR complexes confirm this coordination environment and demonstrate that the copper is unequivocally in the +1 oxidation state (*21*). The metal-binding domain in Ag^+-CueR and Au^+-CueR is identical to that found in Cu^+-CueR, except for longer metal-sulfur bond distances (Ag-S: 2.35 Å; Au-S: 2.32 and 2.39 Å). All sulfur-to-metal distances and bond angles (176° to 177°) are consistent with the average values for linear, two-coordinate Cu^+, Ag^+, and Au^+ complexes found in the small-molecule Cambridge Structural Database.

Mutation of Cys[112] or Cys[120] in CueR abrogates all response to Cu^+, Ag^+, and Au^+ in vivo (*12*) and in vitro (*21*), and the structure confirms that the surrounding environment does not allow for other types of interactions with the metal. The closest residue with metal-binding potential is Ser[77] from the second monomer, which has a Cu-Oγ distance (4.4 Å) that is too long for primary or secondary covalent-bonding interactions. Instead, Ser[77] is within hydrogen-bonding distance to Asp[115] and several main-chain atoms of the metal-binding loop (Fig. 3, A and B). These interactions may be important in maintaining the conformation of the metal-binding loop and stabilizing the quaternary interactions in the dimer interface.

The overall structure of the truncated ZntR dimer is similar to that of CueR and consists of one helix-turn-helix motif of the DNA-binding domain, the dimerization helix, and an intact metal-binding domain. In ZntR, both metal-binding domains are well ordered with two Zn^{2+} ions bound at each site through Cys[114], Cys[115], His[119], Cys[124], and Cys[79] (Fig. 3A), which is supported by biochemical data showing a diminished response to Zn^{2+} upon mutation of any of these residues (*22*). The dinuclear Zn-binding site shows each Zn^{2+} ion in a tetrahedral coordi-

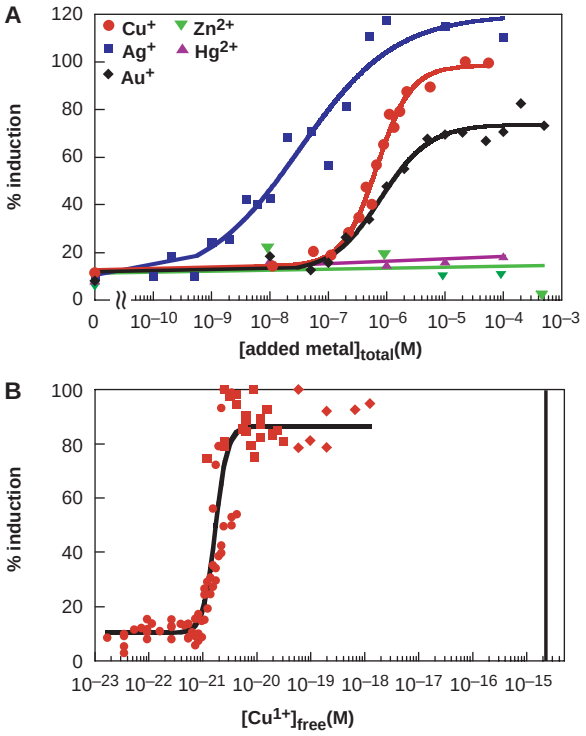

Fig. 1. Metal selectivity and sensitivity of CueR in transcriptional regulation of *copA* in vitro. The incubation buffer (pH 8.0) was treated with Chelex to remove exogenous metals. Concentrations used were as follows: CueR, 50 nM; RNAP, 5 nM; and DTT, 1 mM. The percentage of induction relative to the maximal induction achieved by Cu^+ (% induction) is plotted as a function of metal concentration ([added metal]). (**A**) The buffer was supplemented with 1.0 mM CN^- to sequester transcription induced by residual copper. The solid lines for Cu^+, Ag^+, and Au^+ represent fits to a sigmoidal function, respectively. Half-maximal transcription was observed at 0.7 ± 0.2 μM total Cu^+, at 0.013 ± 0.009 μM total Ag^+ and at 0.6 ± 0.3 μM total Au^+. (**B**) The free Cu^+ concentration ($[Cu^+]_{free}$) was buffered by 20 mM CN^- (circles), 5.0 mM CN^- (squares), and 1.0 mM CN^- (diamonds), respectively (*16*). The vertical line represents the free Zn^{2+} concentration that induces half-maximal transcription of the ZntR/promoter system (*1*).

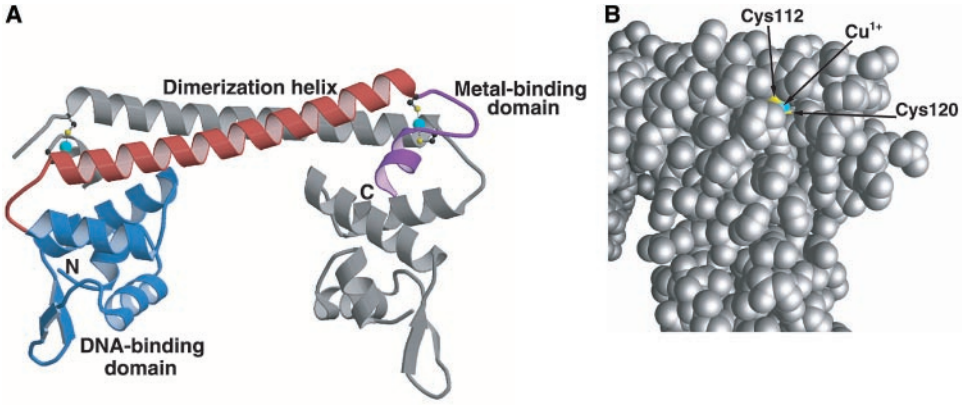

Fig. 2. (**A**) Overall structure of the Cu-CueR dimer. The ribbon diagram depicts one monomer in gray and the functional domains in the other monomer in color, with the DNA-binding domain in blue, the dimerization helix in red, and the metal-binding domain in purple. The N-terminal DNA-binding domain consists of two helix-turn-helix motifs and a three-stranded antiparallel β sheet. The second helix-turn-helix motif of the DNA-binding domain is followed by a five-residue loop connecting to a 10-turn α helix. This long α helix links the DNA-binding domain to the metal-binding domain and contributes to the bulk of the dimerization interface by forming an antiparallel coiled coil with the equivalent helix of the other monomer. The copper ions are shown as cyan spheres, and the coordinating cysteines, Cys[112] and Cys[120], are highlighted in ball-and-stick representation. Most of the metal-binding loop of one monomer (residues 115 to 119) and the last eight residues at the C-termini of both monomers are disordered and are not included in the model. (**B**) A space-filling model of CueR reveals the solvent inaccessibility of the bound metal. The protein is shown in gray and its orientation is similar to that used in (A). The sulfur atoms of the cysteine ligands are colored yellow, and the buried Cu^+ ion is depicted in blue.

nation environment with a Zn-Zn distance of 3.6 Å. Cys^{114} and Cys^{124} (equivalent to Cys^{112} and Cys^{120} in CueR) serve as ligands to Zn1, whereas Cys^{115} and His^{119} coordinate Zn2. Cys^{79} (equivalent to Ser^{77} in CueR) from the other monomer acts as a bridging ligand to the two Zn^{2+} ions, thus linking the metal-binding domain of one monomer and the dimerization domain of the other monomer. An oxygen atom of a bridging phosphate or sulfate group acts as a fourth ligand to each Zn^{2+} ion. In contrast to the CueR metal-binding site, the coordination environment of the metal-binding loop in ZntR is optimal for binding of divalent metals.

The crystal structures of CueR and ZntR reveal several determinants of metal-ion selectivity. A residue at the N-terminus of the dimerization helix extends across the dimer interface to contact either the metal-binding loop (Ser^{77} in CueR) or directly to the metal ion (Cys^{79} in ZntR) and plays a unique role in discriminating between +1 and +2 ions (Fig. 3). A serine is found at this position in all MerR homologs responsive to +1 ions, whereas a cysteine is present in homologs that are known to respond to +2 ions (Fig. 4). Because +2 metal ions typically prefer higher coordination numbers than +1 ions of the coinage metals, discrimination is first conferred at the level of coordinate-covalent bond formation. Second, CueR restricts the bound metal to a low coordination number by hydrophobic and steric restrictions, which contribute to a shielded coordination environment.

Electrostatic features of the metal receptor cavity are the third contributing factor in defining the extraordinary metal affinity and selectivity. In CueR, the buried S-Cu-S center formally has a net negative charge arising from two thiolate anions and one +1 charged metal. The structure reveals a series of weak interactions that compensate this buried charge and provide an electrostatic component to the metal-binding free energy beyond the Cu-S bond energy (Fig. 3, B and C). Charge neutralization of the thiolate of Cys^{120} likely arises from interactions with the positively charged end of the helix dipole and two backbone H bonds that originate from the short two-turn α helix extending from the metal-binding loop. In CueR, Pro^{121} constrains the S atom of Cys^{120} such that it is centered directly over the N-terminus of the short helix (Fig. 3C). A Cys-Pro motif at the N-terminus of an α helix allows for favorable interactions of the cysteine with the helix dipole (*23*), and such a motif is conserved at the end of the metal-binding loop in many of the MerR family members (Fig. 4). Mutation of this proline diminishes the Hg^{2+} response of MerR, consistent with a key role for the Cys-Pro motif (*24*). Cys^{112} accepts only one hydrogen bond (Fig. 3B) and the closest positively charged residue is a conserved lysine, Lys^{81} (the Nζ-S distance is 5.5 Å). The charge-charge interaction of Lys^{81} with the Cys^{112} thiolate, although distant, could contribute additional charge neutralization. These electrostatic- and hydrogen-bonding interactions lead to charge neutrality when a +1 ion, but not a +2 ion, binds. This allows CueR to discriminate against Hg^{2+}-binding in what is otherwise a stable linear dithiolate Hg-coordination environment.

A structure-based sequence alignment of MerR metalloregulatory homologs allows for predictions of metal selectivity in other family members (Fig. 4). A serine or cysteine at the N-terminal end of the dimerization helix provides a clear distinction between putative +1 and +2 metal-responsive subgroups within the MerR family. In the case of PmtR, a role in Zn^{2+} homeostasis has been proposed (*25*); however, the structure-based alignment (Fig. 4) suggests a role in Cu^{+} regulation. For SoxR, a MerR homolog that uses an Fe-S cluster to sense oxida-

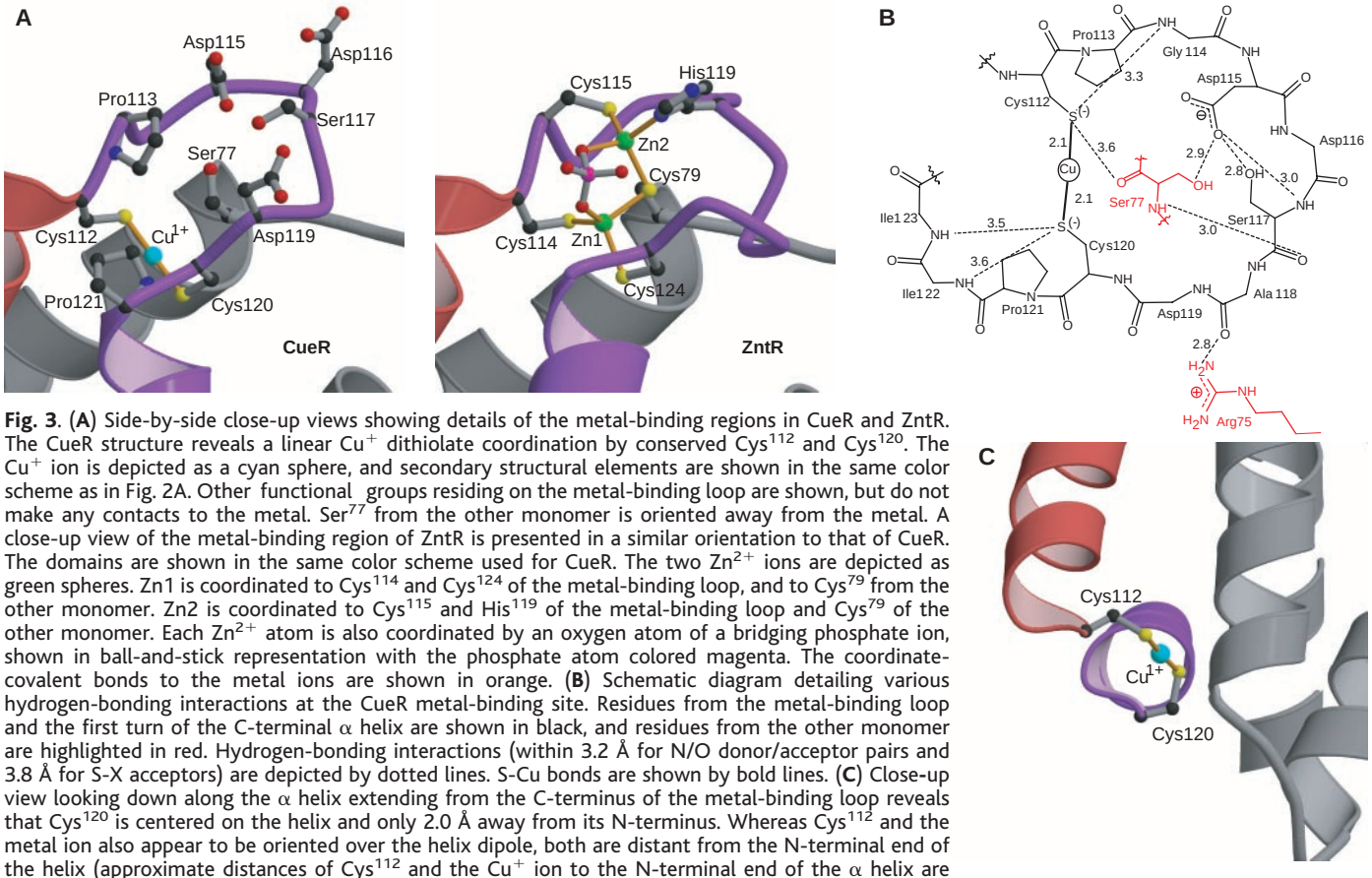

Fig. 3. (**A**) Side-by-side close-up views showing details of the metal-binding regions in CueR and ZntR. The CueR structure reveals a linear Cu^{+} dithiolate coordination by conserved Cys^{112} and Cys^{120}. The Cu^{+} ion is depicted as a cyan sphere, and secondary structural elements are shown in the same color scheme as in Fig. 2A. Other functional groups residing on the metal-binding loop are shown, but do not make any contacts to the metal. Ser^{77} from the other monomer is oriented away from the metal. A close-up view of the metal-binding region of ZntR is presented in a similar orientation to that of CueR. The domains are shown in the same color scheme used for CueR. The two Zn^{2+} ions are depicted as green spheres. Zn1 is coordinated to Cys^{114} and Cys^{124} of the metal-binding loop, and to Cys^{79} from the other monomer. Zn2 is coordinated to Cys^{115} and His^{119} of the metal-binding loop and Cys^{79} of the other monomer. Each Zn^{2+} atom is also coordinated by an oxygen atom of a bridging phosphate ion, shown in ball-and-stick representation with the phosphate atom colored magenta. The coordinate-covalent bonds to the metal ions are shown in orange. (**B**) Schematic diagram detailing various hydrogen-bonding interactions at the CueR metal-binding site. Residues from the metal-binding loop and the first turn of the C-terminal α helix are shown in black, and residues from the other monomer are highlighted in red. Hydrogen-bonding interactions (within 3.2 Å for N/O donor/acceptor pairs and 3.8 Å for S-X acceptors) are depicted by dotted lines. S-Cu bonds are shown by bold lines. (**C**) Close-up view looking down along the α helix extending from the C-terminus of the metal-binding loop reveals that Cys^{120} is centered on the helix and only 2.0 Å away from its N-terminus. Whereas Cys^{112} and the metal ion also appear to be oriented over the helix dipole, both are distant from the N-terminal end of the helix (approximate distances of Cys^{112} and the Cu^{+} ion to the N-terminal end of the α helix are ~6.5 and 4.0 Å, respectively). Structural elements and bonds are colored using the same scheme as in Fig. 2A, and the metal-binding loop has been omitted for clarity.

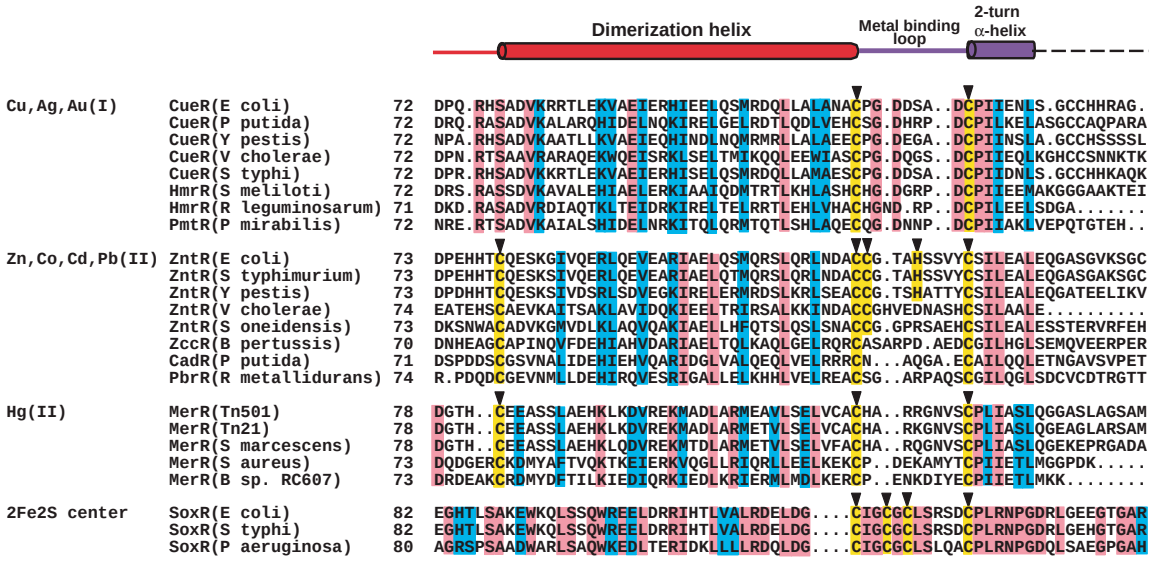

Fig. 4. Structure-based alignment of sequences corresponding to the dimerization and metal-binding domains of various metalloregulatory MerR family members. The sequences of *E. coli* CueR and ZntR were aligned on the basis of structural similarities revealed upon superposition of the crystal structures. Secondary structural elements are shown above the alignment using the same domain color scheme as in Fig. 2A. CueR and ZntR homologs were classified based on sequence similarity, particularly in the metal-binding region. Relevant metal inducer(s) for each +1 and +2 subgroup are listed to the left of the alignment, except for SoxR, which responds to oxidative stress using an Fe-S cluster. Residues that bind metal in the CueR and ZntR structures or are predicted to bind metal in other members are highlighted in yellow and marked by black arrowheads above each subgroup. Identical residues within each subgroup are highlighted in pink, and conserved residues are colored in blue. The alignment shows how proteins responding to +1 ions share a unique signature SerXXVal(Lys/Arg) (where X is any amino acid) at the N-terminal region of the dimerization helix, a CysXGlyX$_4$AspCys metal-binding loop followed immediately by a Pro, which is the N1 residue of the next helix. Alternative signatures are found for members responding to +2 ions. The Hg^{2+}-sensing proteins are predicted to have a Cys at the N-terminus of the dimerization helix and a CysX$_8$Cys loop also followed by a Pro as the first residue in a helix. The Zn^{2+}-sensing proteins have a Cys at the N-terminus of the dimerization helix followed by a CysX$_9$Cys motif with no Pro following the last Cys. Finally, SoxR appears to have a shorter dimerization helix followed by a CysX$_{10}$Cys loop containing no Pro residues, but an additional CysXCys motif characteristic of Fe-S–binding sites in other proteins.

tive stress (*26*), the alignment suggests that the 2Fe-2S cluster will bind in a loop resembling the ZntR binuclear Zn^{2+} site. Furthermore, the ZntR structure reveals how the prototypical metalloregulatory protein in this family, MerR (*27*), could bind Hg^{2+} using a trigonal metal-thiolate coordination environment (*28*) involving two cysteines from one monomer and a third cysteine, the equivalent to Cys^{79} in ZntR, from the other monomer (*24*, *29*–*31*).

The combination of thermodynamic and structural studies reveals how metalloregulatory proteins can select among +1 and +2 transition-metal ions. The extraordinary copper sensitivity of CueR suggests that the prokaryotic cytoplasm operates under conditions of copper deprivation. Given the absence of known copper chaperones in *E. coli*, these results raise the question of how bacterial copper-dependent proteins obtain their cofactor. All copper-dependent enzymes known to date in *E. coli* are found in the cell envelope (*3*, *32*–*36*). The answer may be that available cytosolic copper ions, bound or free, are detected by Cu^+ sensors and rapidly transported to the cell envelope for incorporation or ejection. In this respect, copper homeostasis in Gram-negative bacteria shows a striking parallel to eukaryotic copper trafficking pathways. Both use a family of homologous copper-specific P-type adenosine triphosphatases to clear rapidly any available copper ions from the cytosol into more specialized compartments: the cell envelope in prokaryotes and the trans-Golgi secretory pathway in eukaryotes (*37*).

References and Notes

1. C. E. Outten, T. V. O'Halloran, *Science* **292**, 2488 (2001).
2. L. A. Finney, T. V. O'Halloran, *Science* **300**, 931 (2003).
3. F. W. Outten, D. L. Huffman, J. A. Hale, T. V. O'Halloran, *J. Biol. Chem.* **276**, 30670 (2001).
4. C. Rensing, B. Fan, R. Sharma, B. Mitra, B. P. Rosen, *Proc. Natl. Acad. Sci. U.S.A.* **97**, 652 (2000).
5. G. Grass, C. Rensing, *Biochem. Biophys. Res. Commun.* **286**, 902 (2001).
6. D. L. Huffman *et al.*, *Biochemistry* **41**, 10046 (2002).
7. F. W. Outten, C. E. Outten, J. A. Hale, T. V. O'Halloran, *J. Biol. Chem.* **275**, 31024 (2000).
8. C. Petersen, L. B. Møller, *Gene* **261**, 289 (2000).
9. J. V. Stoyanov, J. L. Hobman, N. L. Brown, *Mol. Microbiol.* **39**, 502 (2001).
10. Y. Hitomi, C. E. Outten, T. V. O'Halloran, *J. Am. Chem. Soc.* **123**, 8614 (2001).
11. D. M. Ralston, T. V. O'Halloran, *Proc. Natl. Acad. Sci. U.S.A.* **87**, 3846 (1990).
12. J. V. Stoyanov, N. L. Brown, *J. Biol. Chem.* **278**, 1407 (2003).
13. Materials and methods are available as supporting material on *Science* Online.
14. A. E. Martell, R. M. Smith, *NIST Critical Stability Constants of Metal Complexes* [National Institute of Standards and Technology (NIST) Standard Reference Database 46, 2001].
15. Extremely high stability constants have been reported for the Cu^+-GSH complexes (*38*). However, different thermodynamic results are indicated by recent spectroscopic studies (*39*).
16. The Cu^+ binding constants (β_n, where $n \geq 2$) and the proton association constant (K) of CN^- at 25°C and 0.1 M ionic strength were obtained from the *NIST Critical Stability Constants of Metal Complexes* (*14*):

$$Cu^+_{free} + 2CN^- \rightleftharpoons [Cu(CN)_2]^- \quad \log\beta_2 = 21.7 \quad (1)$$

$$Cu^+_{free} + 3CN^- \rightleftharpoons [Cu(CN)_3]^{2-} \quad \log\beta_3 = 26.8 \quad (2)$$

$$Cu^+_{free} + 4CN^- \rightleftharpoons [Cu(CN)_4]^{3-} \quad \log\beta_4 = 27.9 \quad (3)$$

$$H^+ + CN^- \rightleftharpoons HCN \quad \log K = 9.04 \quad (4)$$

At a given total Cu^+ concentration, the free Cu^+ concentration at pH 8.0 was calculated with $[CN^-]_{total}$, $[Cu^+]_{total}$, and the above constants using the HySS program (*40*) (fig. S2). Considering the metal-buffering capacity of a given ligand concentration, only the free Cu^+ concentration ranges that can be precisely controlled by the chosen ligand system (fig. S2, highlighted in gray) were used in the experiments shown in Fig. 1B.
17. K. Chen and T.V. O'Halloran, data not shown.
18. E. E. Heldwein, R. G. Brennan, *Nature* **409**, 378 (2001).
19. M. H. Godsey, N. N. Baranova, A. A. Neyfakh, R. G. Brennan, *J. Biol. Chem.* **276**, 47178 (2001).
20. Superposition of the CueR DNA binding and dimerization core with that of BmrR [Protein Data Bank (PDB) accession code 1EXJ] and MtaN (PDB accession code 1JBG) reveals a root mean square deviation for Cα atoms of 1.64 and 1.46 Å, respectively.
21. K. Chen, S. Yuldasheva, J. E. Penner-Hahn, T. V. O'Halloran, *J. Am. Chem. Soc.*, in press.
22. S. Khan, K. R. Brocklehurst, G. W. Jones, A. P. Morby, *Biochem. Biophys. Res. Commun.* **299**, 438 (2002).
23. T. Kortemme, T. E. Creighton, *J. Mol. Biol.* **253**, 799 (1995).
24. W. Ross, S.-J. Park, A. O. Summers, *J. Bacteriol.* **171**, 4009 (1989).
25. M. Noll, K. Petrukhin, S. Lutsenko, *J. Biol. Chem.* **273**, 21393 (1998).
26. B. Demple, H. Ding, M. Jorgensen, *Methods Enzymol.* **348**, 355 (2002).
27. T. V. O'Halloran, C. Walsh, *Science* **235**, 211 (1987).
28. L. M. Utschig, J. W. Bryson, T. V. O'Halloran, *Science* **268**, 380 (1995).
29. L. M. Shewchuk *et al.*, *Biochemistry* **28**, 2340 (1989).
30. J. D. Helmann, B. T. Ballard, C. T. Walsh, *Science* **247**, 946 (1990).
31. J. G. Wright, H.-T. Tsang, J. E. Penner-Hahn, T. V. O'Halloran, *J. Am. Chem. Soc.* **112**, 2434 (1990).
32. J. Abramson *et al.*, *Nature Struct. Biol.* **7**, 910 (2000).
33. C. M. Wilmot, J. Hajdu, M. J. McPherson, P. F. Knowles, S. E. V. Phillips, *Science* **286**, 1724 (1999).
34. J. H. Roh, Y. Takenaka, H. Suzuki, K. Yamamoto, H. Kumagai, *Biochem. Biophys. Res. Commun.* **212**, 1107 (1995).
35. A. Pesce *et al.*, *J. Mol. Biol.* **274**, 408 (1997).

36. S. A. Roberts *et al.*, *Proc. Natl. Acad. Sci. U.S.A.* **99**, 2766 (2002).
37. T. V. O'Halloran, V. C. Culotta, *J. Biol. Chem.* **275**, 25057 (2000).
38. R. Österberg, R. Ligaarden, D. Persson, *J. Inorg. Biochem.* **10**, 341 (1979).
39. A. Corazza, I. Harvery, P. J. Sadler, *Eur. J. Biochem.* **236**, 697 (1996).
40. Alderighi *et al.*, *Coord. Chem. Rev.* **184**, 311 (1999).
41. We thank C. Fahrni, L. A. Finney, H. A. Godwin, E. Kawamoto, and J. L. Wolford for helpful discussions. Supported by NIH GM51350 (to A.M.), NIH GM38784 (T.V.O.), NIH F32 DK61868 (K.C.), and the National Research Service Award Institutional Training Grant in Molecular Biophysics (NIH GM08382) (A.C. and C.E.O.). We acknowledge the use of instruments in the Keck Biophysics Facility at Northwestern University. Support from the R.H. Lurie Comprehensive Cancer Center of Northwestern University to the Structural Biology Facility is acknowledged. Portions of this work were performed at the DuPont-Northwestern-Dow Collaborative Access Team (DND-CAT) Synchrotron Research Center at the Advanced Photon Source (APS) and at the Stanford Synchrotron Radiation Laboratory (SSRL). DND-CAT is supported by DuPont, Dow, the state of Illinois, and the NSF, and use of the APS is supported by the U.S. Department of Energy (DOE). SSRL is operated by the DOE, Office of Basic Energy Sciences. The SSRL Biotechnology Program is supported by the NIH and the DOE. Coordinates and structure factors have been deposited in the Protein Data Bank with accession numbers 1Q05, 1Q06, 1Q07, 1Q08, 1Q09, and 1Q0A.

Supporting Online Material
www.sciencemag.org/cgi/content/full/301/5638/1383/DC1
Materials and Methods
Figs. S1 and S2
Table S1
References

21 April 2003; accepted 28 July 2003

Autophagy Genes Are Essential for Dauer Development and Life-Span Extension in *C. elegans*

Alicia Meléndez,[1] Zsolt Tallóczy,[1] Matthew Seaman,[2] Eeva-Liisa Eskelinen,[3] David H. Hall,[4] Beth Levine[1]*

Both dauer formation (a stage of developmental arrest) and adult life-span in *Caenorhabditis elegans* are negatively regulated by insulin-like signaling, but little is known about cellular pathways that mediate these processes. Autophagy, through the sequestration and delivery of cargo to the lysosomes, is the major route for degrading long-lived proteins and cytoplasmic organelles in eukaryotic cells. Using nematodes with a loss-of-function mutation in the insulin-like signaling pathway, we show that *bec-1*, the *C. elegans* ortholog of the yeast and mammalian autophagy gene *APG6/VPS30/beclin1*, is essential for normal dauer morphogenesis and life-span extension. Dauer formation is associated with increased autophagy and also requires *C. elegans* orthologs of the yeast autophagy genes *APG1*, *APG7*, *APG8*, and *AUT10*. Thus, autophagy is a cellular pathway essential for dauer development and life-span extension in *C. elegans*.

Under conditions of high population density, limited food, or increased temperature, *Caenorhabditis elegans* nematodes reversibly arrest in an alternate third larval stage, the dauer diapause, which is specialized to survive in an unfavorable environment (*1*). Entry into dauer is regulated by different signaling pathways, including transforming growth factor (TGF-β), cyclic guanosine monophosphate, and insulin-like signaling. Single-gene mutations in the insulin-like signaling pathway that promote constitutive dauer phenotypes also prolong adult life-span (*2*). Despite extensive characterization of regulatory signals, the cellular pathways involved in dauer morphogenesis and longevity are not well understood.

The regulation of dauer entry in *C. elegans* shares similarities with the induction of autophagy in other eukaryotes. The environmental cues that promote dauer morphogenesis in *C. elegans* are also potent stimulators of autophagy in yeast and mammalian cells (*3*, *4*). Through autophagy, cells generate sufficient pools of amino acids to synthesize proteins that are essential for survival when the environmental food supply is limited. Components of the insulin-like signaling pathway that positively (e.g., *daf-18*) and negatively (e.g., *age-1* and *akt1/akt2*) regulate dauer entry in *C. elegans* may also regulate autophagy in mammalian cells (*5*, *6*). Furthermore, autophagy may be involved in life-span extension induced by dietary restriction in mammals (*7*), in delaying leaf senescence (*8*, *9*), and in developmental processes that require extensive cellular and tissue remodeling (*10*). We therefore postulated that autophagy is essential in both dauer development and life-span extension in *C. elegans*.

To test this, we used RNA interference (RNAi) (*11*) to inhibit autophagy genes in *C. elegans* that carry a loss-of-function mutation in *daf-2*, the *C. elegans* insulin-like tyrosine kinase receptor (*12*). *daf-2(e1370)* animals are temperature-sensitive *daf-c* class mutants (*13*), with inappropriate constitutive dauer entry at 25°C and extended adult life-span at lower temperatures (such as 15° to 22.5°C) (*12*, *14*) that allow reproductive growth. *C. elegans* contains candidate homologs of several yeast autophagy (*APG*) genes. We focused on *bec-1*, the *C. elegans* ortholog (T19E7.3) of yeast *APG6/VPS30*, because its mammalian counterpart, *beclin 1*, is important in autophagy, embryonic development, and tumor suppression (*15*, *16*). In both yeast and mammalian cells, Apg6/Vps30/Beclin 1 is part of a Class III phosphatidylinositol 3-kinase complex that is thought to be important in mediating localization of other Apg proteins to preautophagosomal structures (*17*, *18*).

C. elegans bec-1 encodes a predicted 375–amino acid, coiled-coil protein that shares 28% homology with yeast Apg6/Vps30p and 31% homology with human Beclin 1. To determine whether *bec-1* is a functional homolog of yeast *APG6/VPS30*, we tested its ability to restore autophagy and vacuolar protein sorting in *APG6/VPS30*-disrupted (Δ*apg6/vps30*) yeast. Using differential interference contrast microscopy, we found that Δ*apg6/vps30* yeast transformed with *C. elegans bec-1* or human *beclin 1*, but not with empty vector, showed an increase in nitrogen starvation–induced autophagy similar to that of Δ*apg6/vps30* yeast transformed with yeast *APG6/VPS30* (Fig. 1A). In contrast, Δ*apg6/vps30* yeast transformed with either *C. elegans bec-1* or human *beclin 1* were unable to properly sort and mature the vacuolar protein carboxypeptidase Y (CPY) (Fig. 1B, top). This defect was not due to a lack of stable *C. elegans* BEC-1 or human Beclin 1 protein expression in yeast (Fig. 1B, bottom) and could not be overcome by overexpression of the Apg6/Vps30p binding partner, Vps38p, that is part of the yeast vacuolar protein sorting complex (*18*) (Fig. 1B, middle). Thus, similar to human *beclin 1* (*15*), *C. elegans bec-1* complements the autophagy but not the vacuolar protein sorting function of *APG6/VPS30* in yeast. In addition, we examined the *C. elegans bec-1* expression pattern using a reporter gene in which the *bec-1* promoter was fused to green fluorescent protein (GFP) coding sequences

[1]Department of Medicine, Columbia University College of Physicians & Surgeons, 630 West 168th Street, New York, NY 10032, USA. [2]Department of Clinical Biochemistry, Cambridge Institute for Medical Research, Addenbrookes Hospital, Cambridge, CB2 2XY, UK. [3]Institute of Biochemistry, University of Kiel, D-24098 Kiel, Germany. [4]Center for *C. elegans* Anatomy, Albert Einstein College of Medicine, Bronx, NY 10461, USA.

*To whom correspondence should be addressed. E-mail: levine@cancercenter.columbia.edu